Physics – Uspekhi **65** (7) 706 – 722 (2022)

INSTRUMENTS AND METHODS OF INVESTIGATION PACS number: 68.35.Gy

Approaches to determining curvature of wafers by their topography

A A Dedkova, I V Florinsky, N A Djuzhev

DOI: https://doi.org/10.3367/UFNe.2021.10.039076

Contents

Abstract. **We discuss peculiarities of the curvature analysis of wafers considering the heterogeneity of their topography for a quantitative estimation and localization of irregularity, or for subsequent calculations of mechanical stresses. We analyze three approaches to calculating surface curvatures from digital elevation models. The first one is based on the analysis of wafer surface profiles using polynomial approximation; the calculation is based on the curvature radius determination of a curved line; mechanical stresses are calculated using the Stoney method. The second approach uses the second partial derivatives of an elevation function in the Cartesian or cylindrical coordinate systems to analyze irregular topography and then to calculate mechanical stresses. The third considers the entire wafer topography as a two-dimensional elevation matrix and uses the mathematical apparatus of differential geometry and the experience of geomorphometry to determine convex and concave areas of the surface as well as to perform a complete analysis of the surface curvature system. We demonstrate the implementation of these approaches on a wafer like a segment of a sphere and on a complex-shaped wafer.**

Keywords: surface, topography, curvature, radius of curvature, deflection, mechanical stresses, deformation, Stoney equation, silicon wafer, optical profilometry, defectiveness, geomorphometry, digital elevation model, DEM

A A Dedkova [(1, a)], **I V Florinsky** [(2, b)], **N A Djuzhev** [(1)]
[(1)] National Research University of Electronic Technology, pl. Shokina 1, 124498 Zelenograd, Moscow, Russian Federation
[(2)] Institute of Mathematical Problems of Biology, Keldysh Institute of Applied Mathematics, Russian Academy of Sciences, ul. Prof. Vitkevicha 1, 142290 Pushchino, Moscow region, Russian Federation
E-mail: [(a)] dedkova@ckp-miet.ru, [(b)] iflor@mail.ru

Received 29 March 2021, revised 5 August 2021
Uspekhi Fizicheskikh Nauk **192** (7) 754 – 771 (2022)
Translated by V L Derbov

1. Introduction

The surface topography analysis of various objects is a widespread problem. Objects of various sizes and origins may be studied, e.g., thin membranes with characteristic dimensions of tens of microns [1], objects like silicon wafers up to 450 mm in diameter, comparable to the dimensions of the human body [2], as well as elements of the geographic shell, i.e., Earth's surface topography in a wide range of scales, from an individual field to regional, continental, and global topography of the land surface and the ocean floor [3].

This paper describes approaches to the calculation of surface curvature from a digital elevation model (DEM) via the example of structures based on silicon wafers. However, the approaches considered apply to any type of object, taking into consideration their specificity.

In controlling wafers, the main goal is often to determine the deflection or curvature radius of the surface. Deflection is the elevation difference between the highest and the lowest surface region. Curvature and curvature radius are mutually reciprocal quantities that characterize a wafer whose shape is similar to that of a spherical segment of the appropriate radius. The obtained data are often used for a quantitative assay of the surface irregularity level and to calculate mechanical stresses.

To determine the curvature radius of a spherical surface, spherometers, autocollimation microscopes, etc. are used [4, 5]. Analyses of more complex-shaped surfaces are carried out using various techniques, frequently optical. The data can be obtained by means of optical profilometry (interferometry) [6–10] by scanning the wafer with a laser beam [11, 12], Makyoh topography [13, 14], coherent gradient sensor (CGS) technology [15–21], or other methods.

Modern analytical equipment allows constructing not only a map of the surface 3D topography, but also maps of surface curvature, including that in specified directions [15–20]. However, such devices are not familiar in industry and are often expensive. Since not every organization can allow itself to purchase new expensive instrumentation in addition to the one of the same type already present, it is of interest to

determine the curvature from the surface shape data obtained using the available equipment.

The goals of the present paper are as follows: (1) to study the basic approaches to the surface elevation map analysis and to the calculation of the curvature radius and curvatures (see Table 1 below); (2) to consider and adapt the appropriate techniques of implementing these approaches in the surface studies of wafers up to 200 mm in diameter; (3) to analyze and evaluate for typical objects the above basic approaches to the surface curvature determination, which allow comparing the samples with each other, constructing curvature distribution maps from wafer DEMs and analyzing them, and using the information obtained to determine mechanical stresses.

2. Determining mechanical stresses based on the surface curvature radius

Since in many cases the wafer curvature is determined to assess mechanical stresses, we dwell on a brief description of such techniques. This will help us to understand the importance of a deep analysis of the wafer surface curvature.

The techniques based on the Stoney equation [22] are widely used thanks to the relative simplicity of their implementation. A structure consisting of a thin film (or a set of thin films) on a substrate is being considered. The basic technique allows calculating the magnitude and the sign of mechanical stresses in the film and the substrate [23]. For the calculation, data on the surface curvature of the round wafer with the film are used. It is worth noting that measurements are often restricted to a surface profile (the line passing through the center of the sample studied [24, 25]), and no analysis of the complete elevation map over the entire sample area is executed. The mechanical stress σ in the film is calculated using the formula

$$\sigma = \frac{E_s d_s^2}{6(1-\nu) d_f R}, \tag{1}$$

where d_f is the film thickness, d_s is the substrate thickness, ν is the substrate Poisson's ratios, E_s is the Young's modulus of a substrate, and R is the effective curvature radius of the substrate. $R = (R_1 R_2)/(R_1 - R_2)$, where R_1 and R_2 are the curvature radii of the substrate wafer before and after the film deposition. In most practical cases, $R_1 \gg R_2$ and $R = R_2$.

Since the deflection h is typically much less than the radius r of the round wafer base, it can be shown by elementary algebra that $R \approx r^2/(2h)$. To calculate mechanical stresses, one can use the expression [26, 27]

$$\sigma = \frac{h E_s d_s^2}{3(1-\nu) d_f r^2}. \tag{2}$$

The technique of calculating mechanical stresses based on the Stoney equation is a subject of intense criticism [15, 28–32] because of substantially simplifying assumptions about the ratio of film and substrate dimensions, ignoring the surface shape irregularity, anisotropy [12], etc. However, thanks to the simplicity and clarity of application, it is still used everywhere [31, 33–40]. There are also a number of studies devoted to the optimization of this technique or to the use of alternative approaches for calculating mechanical stresses based on surface shape data [15, 31, 41–49]. A majority of them use for the calculation the values of curvature, surface curvature radius, or deflection [15, 30, 41–54]. Thus, determining the surface curvature from the data on its shape becomes a primary task.

Expressions (1) and (2) allow calculating the magnitude of mechanical stresses. The assessment result is mainly a numerical value of the mean mechanical stress in the layer on the wafer. However, for a correct comparison of different samples, a unified technique of determining the curvature radius from the surface topography (elevation map) is required. When using the measuring equipment software, the operator manually chooses the region to determine the deflection and to calculate the curvature radius. This approach can hardly be considered optimal, since, in the process of measuring different samples by different operators, the chosen profile regions can differ, and so can the values of the curvature radius finally obtained.

At that, in many cases the wafer surface shape does not fit its ideal representation as a spherical segment (Fig. 1). The shape features that turn out to be beyond the measurement region are also not considered in the analysis of the surface profile. This testifies to the importance of considering the wafer's entire area in the analysis and calculating mechanical stresses by means of expressions allowing for topography irregularities. Using such an approach, one can judge the distribution of mechanical stress over the wafer.

This information can be used to localize areas with the required values of mechanical stresses and areas where the values of mechanical stresses are beyond the technological tolerance. Hence, it becomes possible to establish a correspondence between the characteristics of the operations of the technological route and the final distribution of valid crystals over the wafer [55], which ultimately makes it possible to adjust the technological means of manufacturing crystals so as to provide a maximal yield of good ones.

3. Equipment and samples

The implementation of the approaches is shown by the example of processing experimental data from a Veeco Wyko NT 9300 profilometer, using the method of vertical scanning interferometry [56–59] to construct the surface DEM. The principle of the instrument operation is based on the interference of a light beam reflected from a reference mirror and the surface of a measured object, recording the interference pattern by means of a CCD camera followed by interference pattern analysis to extract quantitative data about the surface shape. White light is used and the position of the maximal-contrast fringe is determined when moving the measuring head along the Z-axis. The equipment allows obtaining DEMs of the structure areas from 47×63 μm to 3.4×4.6 mm in size with the grid size (resolution) from 98 nm to 57 μm. Using the stitching technique, which consists of joining a series of individual data frames, a DEM of larger-area objects is formed (the movable stage of the instrument restricts the scanned region length to 200 mm). To obtain DEMs of the wafers 100–200 mm in diameter, measurements are performed at the nodes of the specified grid using the technique described in Ref. [56].

To measure large-size objects, systems with an automated object stage are used, which move the visual field and then stitch the image frames [60–62]. In this case, even using an optical microscope, one can detect the elevation difference of the structures (by the focus position [63, 64]). Therefore, even in the case of an initially absent stitching module, the upgrade

of the available equipment and obtaining a complete surface elevation map are possible.

Studies were performed with silicon oxide-on-silicon (SiO_2-on-Si) structures produced at the Novellus setups (USA) using PECVD (Plasma Enhanced Chemical Vapor Deposition) deposition and SVCS (Czechia) using CVD (Chemical Vapor Deposition) deposition.

Gas-phase deposition can be defined as condensation of gaseous (vaporous) elements or compounds on substrates with the formation of solid precipitates. In the CVD, the gas phase composition substantially differs from the precipitate composition. The volatile compound of the deposited element is supplied to the substrate, where it is subjected to thermal decomposition (pyrolysis) or participates in reduction chemical reactions with other gases (or vapors), while non-volatile reaction products sediment on the substrate surface.

The precipitates are formed as a result of multiple chemical reactions that take place in the gas phase near the substrate surface and on the surface itself, which highly complicates the deposition process but makes it more universal and flexible. The CVD processes are sometimes referred to as reactive deposition from the gas (gas–vapor, vapor) phase.

CVD is a universal and energy-saving method of atomic/molecular formation of coatings by controlled deposition of a substance in the form of individual atoms or molecules in order to obtain films with the required properties (density, thickness, orientation, composition, etc.). In CVD, the material is deposited in the form of a powder if the reaction of formation of its particles occurs only in the gas phase, and in the form of a film coating, if the solid particles are produced on the substrate surface. Obviously, to fabricate functional layers for an integrated circuit chip, only the second group of CVD processes can be used [65].

CVD processes are implemented using facilities that have a reactor chamber. With respect to the operating pressure in the reactor, the CVD processes are divided into four large groups:

- atmospheric pressure (AP CVD): 760 Torr = 101.3 kPa;
- subatmospheric pressure (SAP CVD): 20–700 Torr = 2.67–93.3 kPa;
- low pressure (LP CVD): $10^{-2}-10$ Torr = 1.33–1333 Pa;
- ultrahigh vacuum (UHV CVD): $10^{-3}-10^{-6}$ Torr = $1.33\times(10^{-1}-10^{-4})$ Pa.

Each of these groups, in turn, is divided into smaller subgroups by the activation method, reagent supply, group of materials to which each deposited layer belongs, and the gas phase chemical composition. Detailed classification of CVD processes with respect to various features used in integrated circuit production is presented in Ref. [65].

To obtain SiO_2 films, three groups of CVD processes are most widely used in technologies for producing integrated circuits and microelectromechanical systems (MEMSs) [65]:

(1) Thermal oxidation in dry or humid oxygen at atmospheric pressure in the temperature range of 900–1100 °C in cylindrical quartz reactors according to the reaction

$$Si + O_2 = SiO_2\,. \qquad (3)$$

In this case, the substrate material (silicon) plays the role of the second reagent in the CVD process.

(2) Thermally stimulated deposition from tetraethoxysilane (TEOS) and oxygen ($Si(OC_2H_5)_4/O_2$), carried out at low pressure ($10^{-2}-10$ Torr) in a temperature range of 650–750 °C in cylindrical quartz reactors evacuated by vacuum pumps according to the reaction

$$Si(OC_2H_5)_4\,(v) + 12O_2\,(g) = SiO_2\,(s) + 10H_2O\,(v) + 8CO_2\,(g)\,, \qquad (4)$$

where the indices (v), (s), and (g) mean vapor, solid film, and gas, respectively.

(3) Plasma enhanced (PE) deposition from the gas mixture of silane (SiH_4) and nitrous oxide (N_2O) using nitrogen (N_2) as a carrier gas, performed at lowered pressures ($10^{-2}-10$ Torr) with switched-on high-frequency (HF) plasma generators with a power of 1.0–2.0 kW in the temperature range of 200–400 °C in planar metallic reactors with ceramic coating evacuated by vacuum pumps according to the reaction

$$SiH_4\,(g) + 2N_2O\,(g) = SiO_2\,(s) + 2N_2\,(g) + 2H_2\,(g)\,. \qquad (5)$$

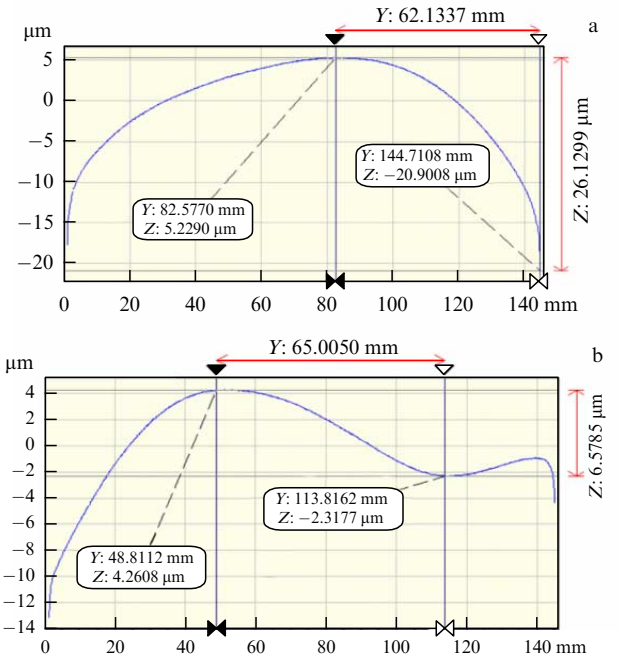

Figure 1. Examples of various shapes of experimental surface profiles of the SiO_2/Si structure. SiO_2 film thickness: (a) 1000 nm and (b) 233 nm.

Examples of various surface profiles are presented in Fig. 1. Shown are the surface profiles of SiO_2/Si wafers formed by PECVD deposition (according to process (5)) of SiO_2 at the temperature of 350 °C on an Si substrate (KDB-12 (100)) 670 μm thick, the thickness of SiO_2 films amounting to 1000 nm (Fig. 1a) and 233 nm (Fig. 1b). The surface profile in Fig. 1a is seen to be much closer to a spherical segment than in Fig. 1b, which is probably a consequence of greater SiO_2 layer thickness (Fig. 1a) formed on an initially irregular wafer.

The implementation of different approaches to wafer DEM processing is illustrated by the example of two different structures: a wafer similar to a spherical segment (Fig. 2a) and a complex-shaped wafer (Fig. 3a). Figure 2a shows an elevation map of the wafer with the SiO_2/Si structure formed by the PECVD deposition of an SiO_2 film 620 nm thick (according to process (5)) on an Si substrate 670 μm thick under the following conditions: time 155 s; consumption of SiH_4 300 $cm^3\ min^{-1}$, of N_2 3000 $cm^3\ min^{-1}$,

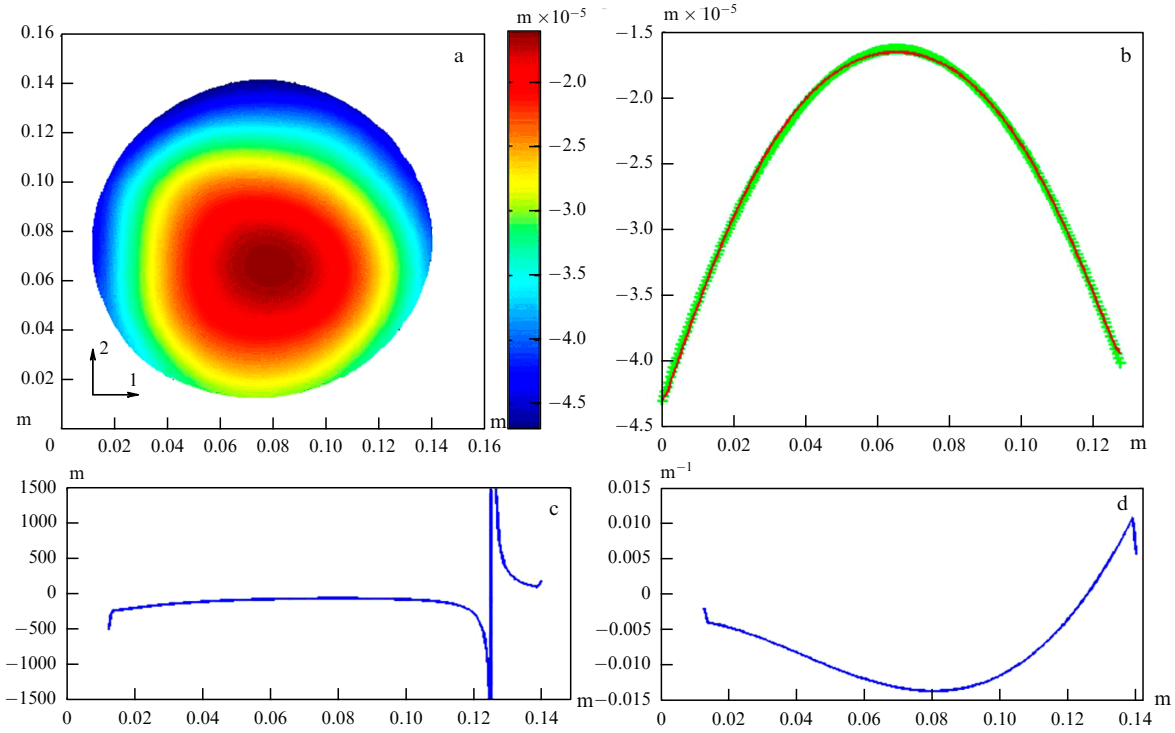

Figure 2. (Color online.) SiO_2/Si structure (wafer shape is close to spherical): (a) wafer surface topography (elevation map), (b) surface profile (red solid line) and corresponding polynomial approximation (green symbols +), (c) distribution of curvature radius values for the profile in Fig. 2b, and (d) distribution of curvature values for the profile in Fig. 2b.

of N_2O 9500 cm^3 min^{-1}; pressure 2.4 Torr, HF generator power 1.1 kW, temperature 270 °C. Figure 3a shows the elevation map of a wafer with the SiO_2/Si structure formed by CVD deposition (according to process (4)) of an SiO_2 film 1250 nm thick on an Si substrate 670 μm thick under the following parameters of the TEOS process: temperature 700 °C, pressure 200 mTorr, consumption of TEOS and oxygen 130 and 40 cm^3 min^{-1}, respectively.

The properties of SiO_2 films, including the type and magnitude of mechanical stresses in them, depend not only on the kind of deposition process but also on the regime parameters of every process, as well as on the thickness of the film deposited or formed on the substrate surface. This applies to films of other materials as well, e.g., silicon nitride (Si_3N_4) deposited on substrates in the course of various CVD processes.

Surface profiles (Figs 2b and 3b) were drawn along the line passing through the wafer center and crossing the base cut.

The use of different techniques to analyze the surface curvature is demonstrated by the example of structures with a smooth surface. However, similar approaches can be used to analyze rough and bumpy surfaces and regions with sharp inhomogeneities. In this case, an important task for the researcher is to construct the DEM correctly and to preprocess it.

4. Determining the curvatures using the formula for planar curves with the polynomial approximation

Hereinafter, experimental data processing is carried out using the programs developed by the authors. The DEMs size is initially 1339 × 1269; after smoothing and demagnification, it becomes 326 × 326.

The experimental data are an array of Cartesian coordinates (x_i, y_i, z_i), where x_i and y_i are planar coordinates of a particular point on the surface, and z_i is the point elevation.

When considering separately each row or column of the elevation matrix Z, surface profiles are in fact selected. Therefore, the data array can be thought of as N vectors $z(x)$, each of dimension M (for profiles parallel to the abscissa x-axis). Such an approach allows applying expressions for planar curves to the curvature calculation.

Curvature $k(x)$ (Table 1) for curve $z = z(x)$ is calculated using the known expression [40, 66, 67]

$$k(x) = \frac{|z''(x)|}{\left[1 + z'^2(x)\right]^{3/2}}. \tag{6}$$

The differentiation is executed using a polynomial approximation. A polynomial $p(x) = p_1 x^n + p_2 x^{n-1} + \ldots + p_n x + p_{n+1}$ is put into correspondence with each curve $z(x)$. The first and second derivatives are calculated using the obtained coefficients $p_1, p_2, \ldots, p_n$.

Since in this case $z_i \ll x_i$, when using a second-order polynomial for approximation, the value of k obtained will not depend on x. Thus, in an analysis of the surface profile $z = z(x)$, only one numerical value of the profile curvature k (and the profile curvature radius $R = 1/k$) will be obtained. The result of such a calculation is independent of the operator and is proposed for use when a simple comparison of samples is needed and for the subsequent calculation of mechanical stresses in the case of a surface shape similar to a sphere segment. In particular, it is proposed to draw profiles $z = z(y)$ and $z = z(x)$ through the wafer center ($N/2$ and $M/2$) and to

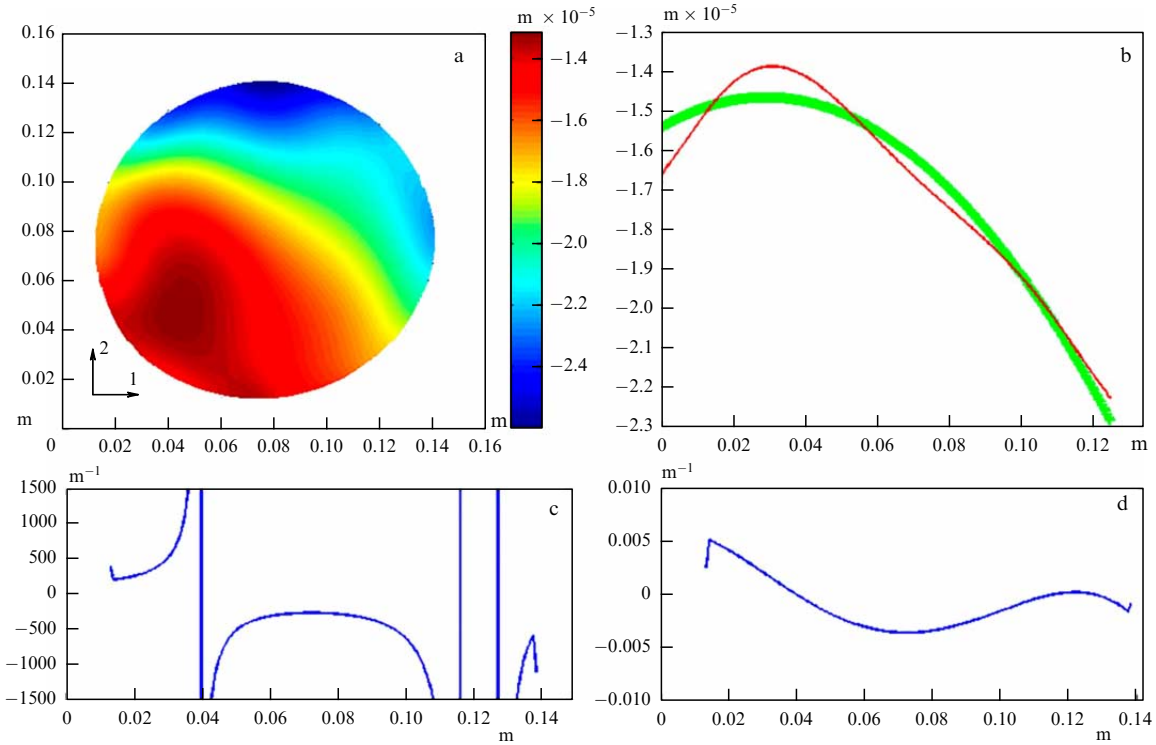

Figure 3. (Color online.) SiO_2/Si structure (complex shape of the wafer): (a) wafer surface topography (elevation map), (b) surface profile (red solid line) and corresponding polynomial approximation (green symbols +), (c) distribution of curvature radius values for the profile in Fig. 3b, and (d) distribution of curvature values for the profile in Fig. 3b.

calculate the corresponding curvature radii using second-order polynomials. In fact, these are profiles along two lines, parallel and perpendicular to the base cut of the wafer, which is most often used in such an analysis [7, 41].

A result of this approach to the analysis of the surface shape of the SiO_2/Si structure is shown in Fig. 2a. The surface profile constructed based on the measurement data and the function approximating it, based on a second-order polynomial, are shown in Fig. 2b. The curves are seen not to coincide ideally with each other; however, the dependence character is similar. The curvature radii for two profiles of the surface parallel to the x- and y-axes turns out to equal -80 and -90 m.

The technique described is efficient for the analysis of wafers, whose deflection shape corresponds of a second-order polynomial, i.e., can be described by a single value of the curvature radius. In most cases, this is so. However, in practice, it is necessary to deal with wafers having a more complex surface shape [11, 13, 14] (Fig. 3a, b). In these cases, it is also possible to use the described technique, but with its approximate character taken into account.

On the other hand, of interest is the possibility of calculating local curvature radii at each point of the surface profile and, based on the obtained data, mapping the surface curvature and, therefore, the mechanical stress distribution over the wafer [18–20, 41, 68, 69]. This would allow localizing regions with acceptable and unacceptable mechanical stress values, as mentioned above.

In addition, such an approach would allow dealing with complex-shaped surface profiles (Fig. 3a, b). Overall, the above technique based on second-order polynomials can be applied to determine local curvature radii using only a small segment of curve $z(x)$ centered at the point of interest. An

Table 1. Some notions used to describe approaches to determining wafer curvature.

Wafer curvature radius	Radius of the sphere segment coincident with the wafer
Wafer curvature	Quantity reciprocal of the curvature radius
Wafer deflection	Difference in elevations between highest and lowest regions of the wafer
Curvature $k(x)$ for curve $z = z(x)$ [40, 66, 67]	$k(x) = \dfrac{\lvert z''(x)\rvert}{\left[1 + z'^2(x)\right]^{3/2}}$
First and second partial derivatives for surface $z = z(x, y)$ in the Cartesian system of coordinates	$k_x = \dfrac{\partial z}{\partial x}$ $k_y = \dfrac{\partial z}{\partial y}$ $k_{xx} = \dfrac{\partial^2 z}{\partial x^2}$ $k_{yy} = \dfrac{\partial^2 z}{\partial y^2}$ $k_{xy} = \dfrac{\partial^2 z}{\partial x \partial y}$
Second partial derivatives for surface $z = z(r, \theta)$ in cylindrical coordinates [79]	$k_{rr} = \dfrac{\partial^2 z}{\partial r^2}$ $k_{\theta\theta} = \dfrac{1}{r}\dfrac{\partial z}{\partial r} + \dfrac{1}{r^2}\dfrac{\partial^2 z}{\partial \theta^2}$ $k_{r\theta} = \dfrac{\partial}{\partial r}\left(\dfrac{1}{r}\dfrac{\partial z}{\partial \theta}\right)$

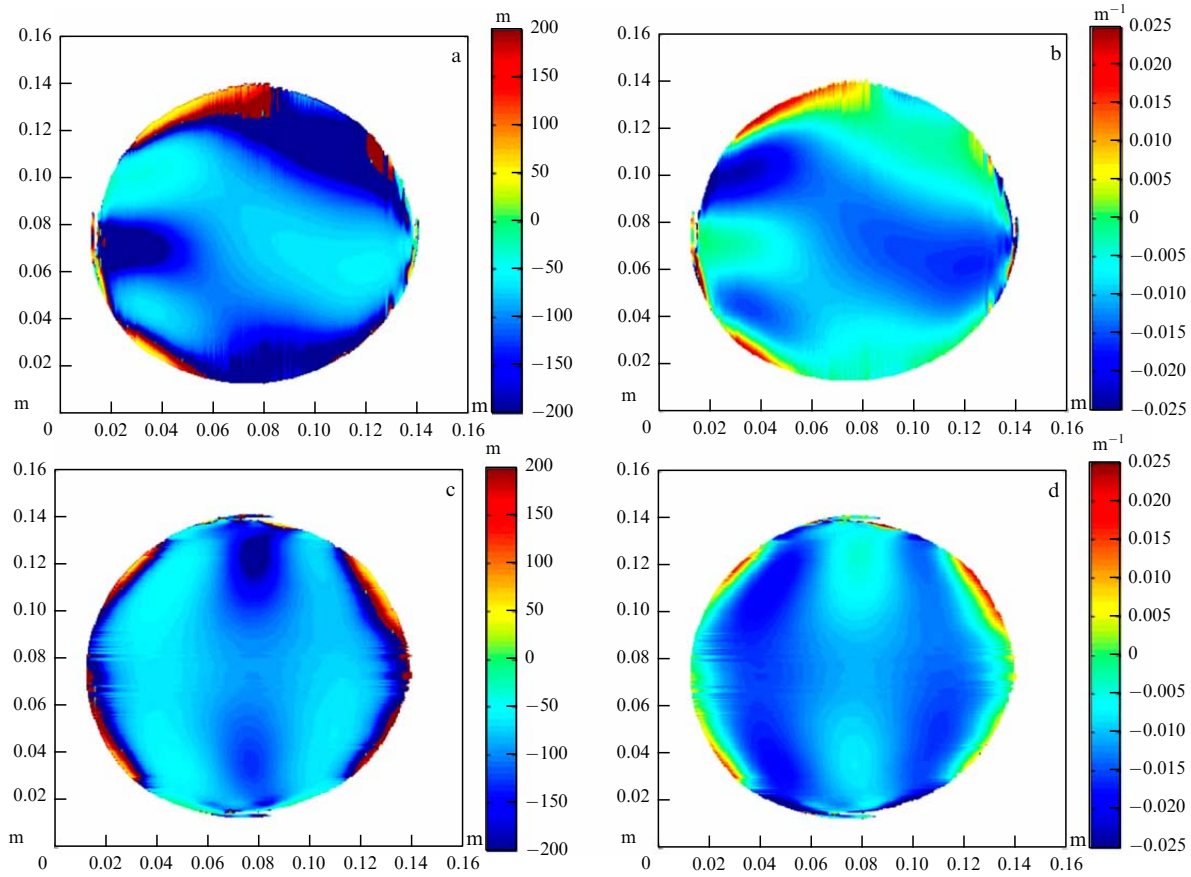

Figure 4. Calculated curvature radius and curvature in two principal directions for the wafer shape close to spherical (topography presented in Fig. 2a): (a) curvature radius in direction 1, (b) curvature in direction 1, (c) curvature radius in direction 2, and (d) curvature in direction 2 (directions are according to Fig. 2a).

alternative option is approximating by higher-degree polynomials [10] followed by the calculation of derivatives taking into account the obtained set of coefficients. According to the authors' experience, the degree of six is typically sufficient; higher degrees of polynomials can be used if necessary.

The obtained dependences of the curvature radius and the curvature itself are presented in Figs 2c, d and 3c, d. The character of these dependences agrees with Figs 2b and 3b, respectively — the position of inflection points, regions of maximal deflection, etc. By performing a similar calculation for all profiles along a certain direction, one can make a map of the curvature radius and surface curvature (Figs 4 and 5).

When drawing the surface profiles, any choice of the direction is possible, not only along the axes x and y. In this case, the initial data arrays (x_i, y_i, z_i) should be used to determine the appropriate coordinates u_i and functions $z(u)$.

Since, due to the anisotropy of mechanical characteristics and nonuniformity of topography, it is generally possible to speak only of the curvature radius and mechanical stresses at a chosen point on the surface in the chosen direction [10, 41, 70], such an approach allows determining the parameters of interest for researchers in various types of structures.

The above techniques are proposed for use when it is necessary to compare samples with each other by one parameter (one value of curvature or curvature radius), to calculate mechanical stresses using the Stoney equation, and to map curvature and curvature radius for a series of profiles, meaning these terms as quantities obtained from Eqn (6) for planar curves.

5. Determining the curvatures by calculating the second partial derivatives, including in the cylindrical coordinates

In the approaches described, the wafer topography is considered as a series of surface profiles. However, for higher-precision analysis, the wafer should be treated as an integral structure, in which the mutual position of convex and concave surface features determines the curvature and, therefore, affects the mechanical stresses in neighboring regions. Moreover, when analyzing a complex surface shape, it is difficult to operate with the notion of surface profiles, since, for each region of analysis, the question of its own optimal choice of profile direction arises.

As was mentioned above, at present, a number of techniques are being developed for calculating mechanical stresses, taking into account the imperfection of the structure considered, including the influence of adjacent regions. In optimized techniques, to derive analytical expressions and perform calculations, the partial derivatives k_{xx}, k_{yy}, and k_{xy} are frequently used (see Table 1) [10, 20, 71–73], which in the special literature are sometimes incorrectly referred to as 'curvature.' The calculation of the array of k_{xx}, k_{yy}, and k_{xy} values from the initial data array (x_i, y_i, z_i) is usually carried out using standard finite-difference approximations of differentiation, implemented in many software packages. Using the values of k_{xx}, k_{yy}, and k_{xy}, they calculate the mechanical stresses [21], taking into account the anisotropy of material characteristics and surface shape.

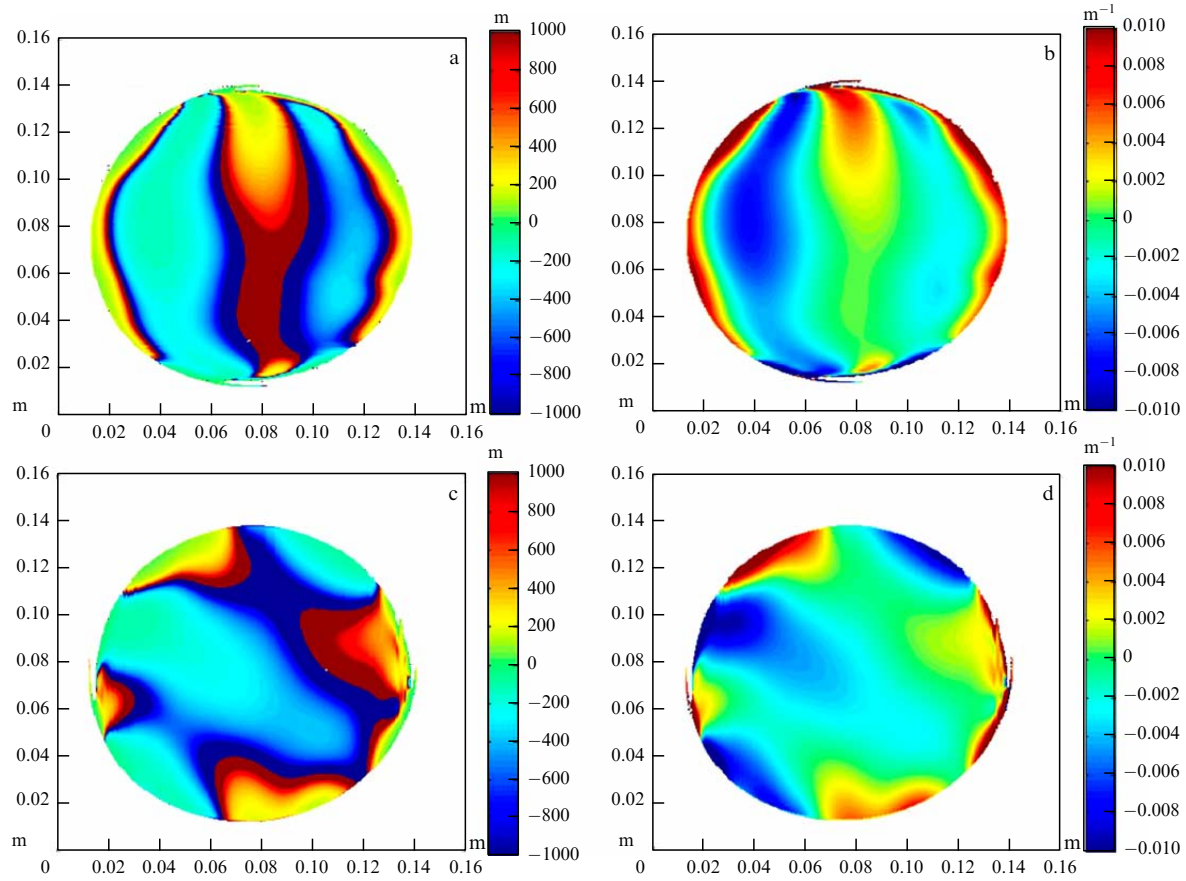

Figure 5. Calculated curvature radius and curvature in two principal directions for a wafer of complex shape (topography presented in Fig. 3a): (a) curvature radius in direction 1, (b) curvature in direction 1, (c) curvature radius in direction 2, and (d) curvature in direction 2 (directions are according to Fig. 3a).

Examples of calculations of k_{xx}, k_{yy}, and k_{xy} for two SiO_2/Si structures (Figs 2a and 3a) are presented in Figs 6 and 7, respectively.

On the whole, since $z_i \ll x_i$, such an approach yields a result similar to the calculation of a map from a series of profiles and polynomials of high degree, described in Section 4. Indeed, the patterns in Fig. 6a are similar to those in Fig. 4b, and the patterns in Figs 6b, 7a, and 7b, to those in Figs 4d, 5b, and 5d, respectively.

However, considering the geometry of the samples studied (round wafers), the calculations are often carried out in cylindrical coordinates rather than in Cartesian ones [74–76]. The technique in Refs [19, 68, 77–79] implies using the CGS method for measurements [15–18, 20, 21], and the processing of experimental data is performed using Zernike polynomials [79–82]. However, having an array of experimental data (x_i, y_i, z_i) obtained by an alternative method, this technique of stress calculation is applied even without using the Zernike polynomials. For this purpose, array (x_i, y_i, z_i) in Cartesian coordinates should be transformed into array (r_i, θ_i, z'_i) in the cylindrical coordinates, and then the partial derivatives should be calculated.

As a rule, the correct transformation of coordinate systems requires preprocessing of the (x_i, y_i, z_i) array. Therefore, in the analysis of round wafers, we leveled the lateral dimensions, moved the wafer center into the image center, smoothed the surface, etc. Since, to calculate derivatives in the cylindrical coordinates, a uniform grid of data (r_i, θ_i) is required, initially such a data set (r_i, θ_i) was specified. Then, it was transformed into Cartesian coordinates (x'_i, y'_i), and then, using the initial values of z_i in the initial experimentally measured Cartesian coordinates (x_i, y_i), the values of z'_i were calculated by means of interpolation.

The calculated second partial derivatives k_{rr}, $k_{\theta\theta}$, $k_{r\theta}$ (see Table 1) for two SiO_2/Si structures (Figs 2a and 3a) are presented in Figs 8 and 9, respectively.

The approaches described in the present section are proposed for use in the correct calculation of normal and shear mechanical stresses using optimized expressions in the case of the anisotropy of the samples studied. Note also that, since in many cases the structures studied possess a central symmetry (spherical shaped wafers, membranes, film isles, etc.), the data representation in cylindrical coordinates can substantially simplify the problem under study.

6. Determining the surface curvatures by calculating the principal curvatures. Geomorphometry

The necessity to operate with three values of second derivatives instead of one value of curvature, to perform rather high volumes of computation work, and to use cylindrical coordinates makes more difficult the widespread acceptance of the approaches described in the previous section. Overall, they are suitable for precise calculation of normal and shear mechanical stresses. However, there is often a problem of assessing the spatial distribution of curvature values of topography inhomogeneities, as well as mechanical stresses over the wafer surface. In this case, it is reasonable to analyze the wafer topography in whole as a

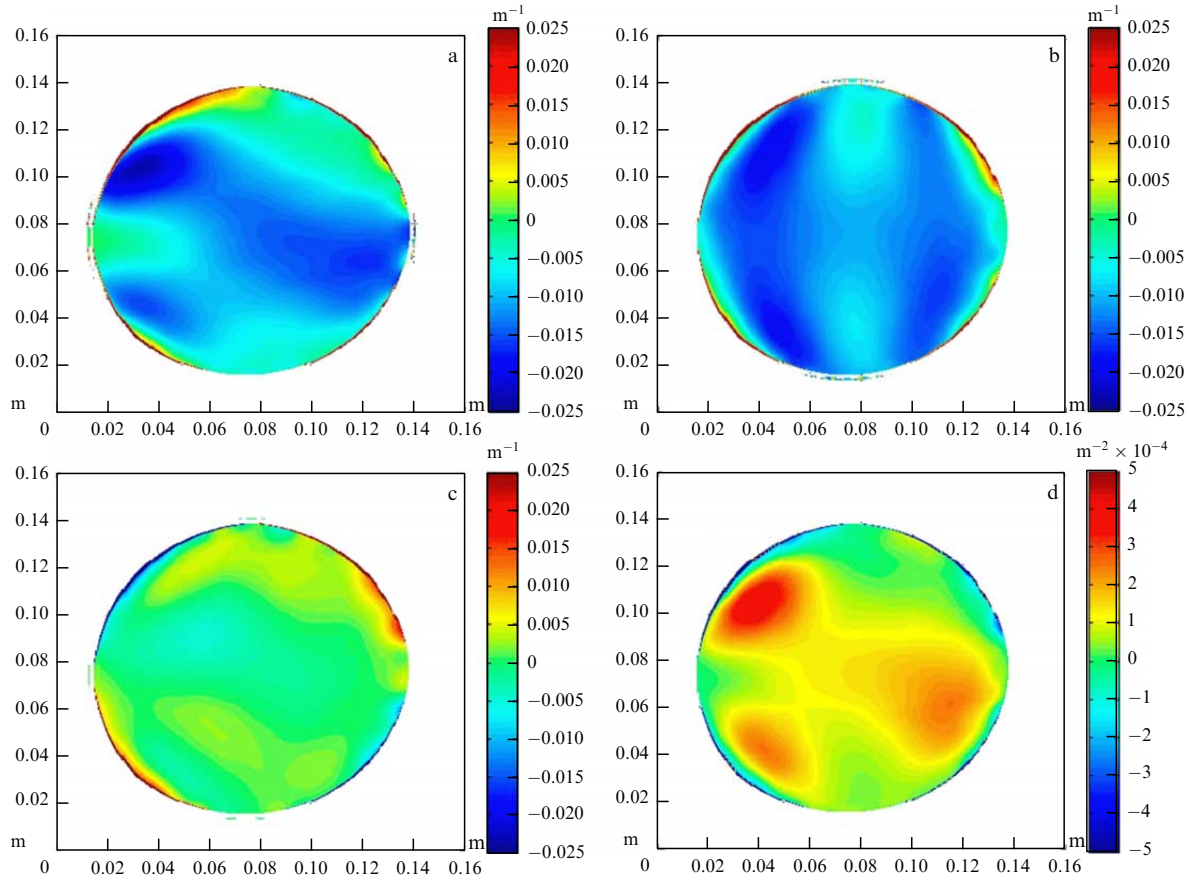

Figure 6. Results of calculations in a Cartesian system of coordinates for the wafer shape close to spherical (topography presented in Fig. 2a): (a) k_{xx}, (b) k_{yy}, (c) k_{xy}, (d) Gaussian curvature approximation $\hat{K} = k_{xx}\,k_{yy} - k_{xy}^2$.

two-dimensional matrix of Z values, i.e., as a DEM rather than a series of profiles.

On the other hand, a detailed analysis of the wafer surface shape can offer a number of data that can be useful, not only for the analysis of mechanical stresses but also for other purposes (e.g., a detailed analysis of volume defects).

From the differential geometry considering a surface in three-dimensional Euclidean space, such notions are well known as principal curvatures, mean curvature, Gaussian (total) curvature, etc. [66, 67, 83–85]. The relative complexity of the mathematical apparatus of this discipline restricts the wide dissemination of the techniques based on it, including in the field of microelectronics. However, practical application of the principles of differential geometry is simple enough to understand, and the performed calculations of curvature from the DEM are trivial and easily implementable in many software environments [86]. In this section, we present a number of data that can be obtained by analyzing the principal curvatures of a surface and related quantities.

It is not an overstatement to say that the notions and mathematical apparatus of the surface theory in differential geometry turn out to be most developed in the physical and mathematical theory of a topographic surface in the gravity field [87, 88], which is a theoretical base for geomorphometry. Geomorphometry is a scientific discipline whose subject is mathematical modeling and analysis of topography, as well as interconnections between the topography and other components of geosystems. At present, geomorphometry is widely used to solve various problems in the Earth sciences [3, 89]. In this connection, it is reasonable to present the approach to determining the curvatures of wafer surfaces through the calculation of principal curvatures based on the fundamentals of the physical and mathematical theory of a topographic surface in a gravity field.

A topographic surface is a closed, oriented, infinitely differentiable two-dimensional manifold S in three-dimensional Euclidean space E^3. A number of restrictions hold, among which, in our case, three are essential [3, 87]:

(1) A topographic surface is defined by a continuous, single-valued bivariate function $z = f(x, y)$, where z is the elevation, and x and y are Cartesian coordinates. This condition notably means that caves, grottos, and similar topography shapes are not considered.

(2) Function $z = f(x, y)$ is smooth, i.e., a topographic surface has derivatives of all orders. In geomorphometry, the first, second, and sometimes third derivatives of the elevation are systematically used.

(3) A topographic surface is a scale-dependent object. This condition means that the 'fractal' topography component can be considered HF noise. In geomorphometry, fractal models, as a rule, are not used.

A morphometric variable is a single-valued bivariate function describing the properties of a topographic surface. A local morphometric variable is a single-valued bivariate function, describing the geometry of the topographic surface in the neighborhood of a given point of the surface along the directions specified by one of the two pairs of mutually perpendicular normal sections (Fig. 10).

The first pair of normal sections is principal sections APA' and BPB', which are well known from differential geometry [85] (Fig. 10a). They are normal sections possessing

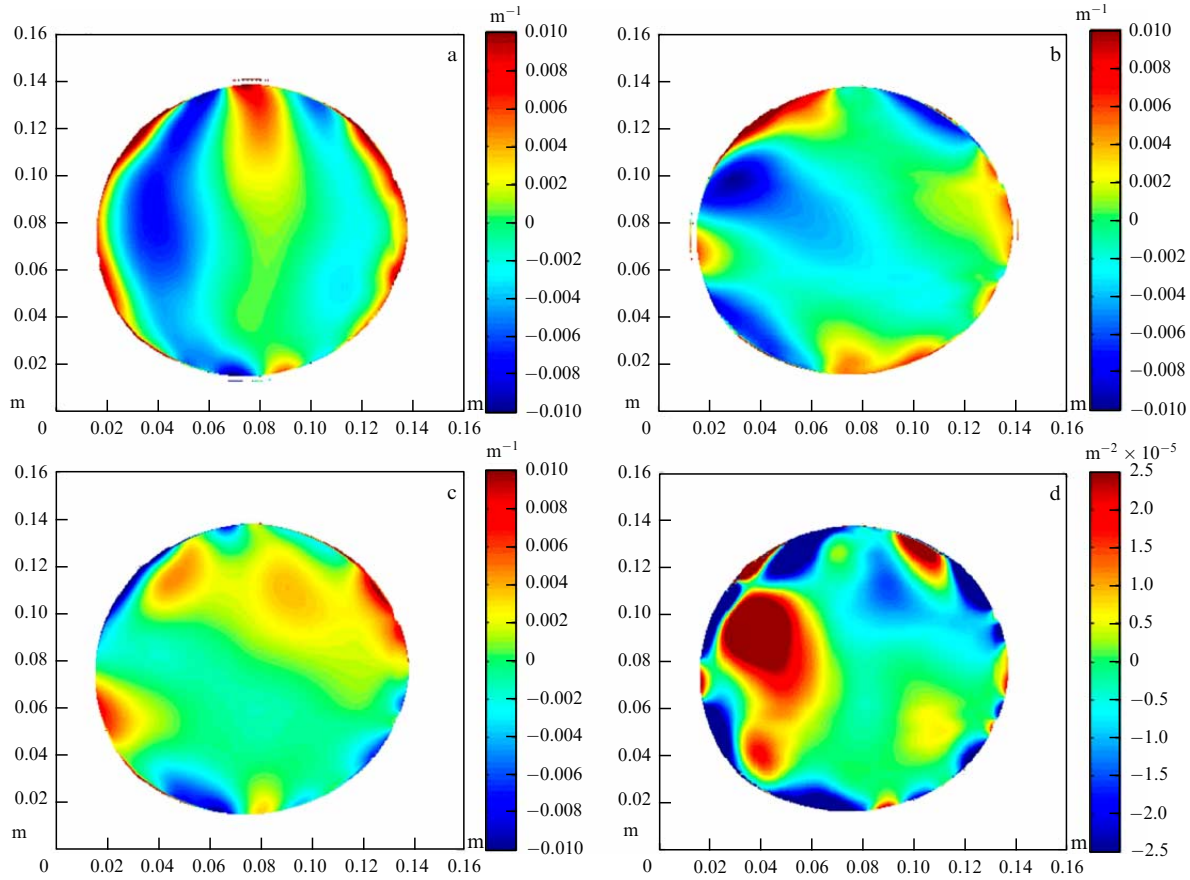

Figure 7. Results of calculations in a Cartesian system of coordinates for the wafer complex shape (topography presented in Fig. 3a): (a) k_{xx}, (b) k_{yy}, (c) k_{xy}, (d) Gaussian curvature approximation $\hat{K} = k_{xx}\,k_{yy} - k_{xy}^2$.

the maximal and minimal bend at a given point P on the topographic surface.

The second pair of normal sections CPC' and DPD' is specified by the gravity field [87] (Fig. 10b). The normal section DPD' contains the vector of the gravity force acceleration **g** and has a common tangent with the slope line at a given point P on the topographic surface. The normal section CPC' is tangent to the contour line at a given point P on the topographic surface.

The two above pairs of normal sections correspond to two classes of local morphometric variables: form attributes and flow attributes [87, 88].

Form attributes are related to principal sections. These variables are gravity field invariants, i.e., they are independent of the direction of the gravity force acceleration. Form attributes include two principal curvatures, the minimal ($k_{\min}$) and the maximal ($k_{\max}$), the mean curvature (H), the Gaussian curvature (K), the unsphericity (M), and some other variables (Table 2).

Flow attributes [1] are related to normal sections, selected by gravity. These variables depend on the direction of the gravity force acceleration vector. The flow attributes include the horizontal curvature ($k_{\rm h}$), the vertical curvature ($k_{\rm v}$), the horizontal excess curvature ($k_{\rm he}$), the vertical excess curvature ($k_{\rm ve}$), the difference curvature (E), the accumulation curvature ($K_{\rm a}$), the ring curvature ($K_{\rm r}$), and some other variables (see Table 2).

The formulas and brief interpretations for 12 local morphometric variables, making up a complete system [2] of curvatures [87], are presented in Table 2. Local topographic characteristics are functions of the elevation partial derivatives. Their calculation from a DEM is performed either by finite-difference methods or by means of the universal spectral analytic method [3].

The surface of any wafer is obviously rough to a certain degree and can have sharp inhomogeneities (defects), i.e., it is not smooth in the mathematical sense and its elevation function can have discontinuities. The initial data for the geomorphometric analysis are DEMs, the single-valued discrete functions of two variables, which describe such roughness and discontinuities in a natural way. The computation algorithms used in geomorphometry allow calculating both partial derivative and curvature models from such DEMs, since they use either a local (within a moving

[1] The commonly accepted term 'flow attributes' was introduced to denote morphometric variables used to analyze lateral flows of a substance (mainly water) moving over the surface and the near-surface layer of Earth subjected to gravity. However, flow attributes are successfully applied for 'fine' analysis of the surface geometry regardless of the presence of any flows on it.

[2] We mean the mathematical completeness of the system of variables, i.e., the possibility of expressing all curvatures of this system in terms of other curvatures of the same system; using any other variables in such operations is redundant.

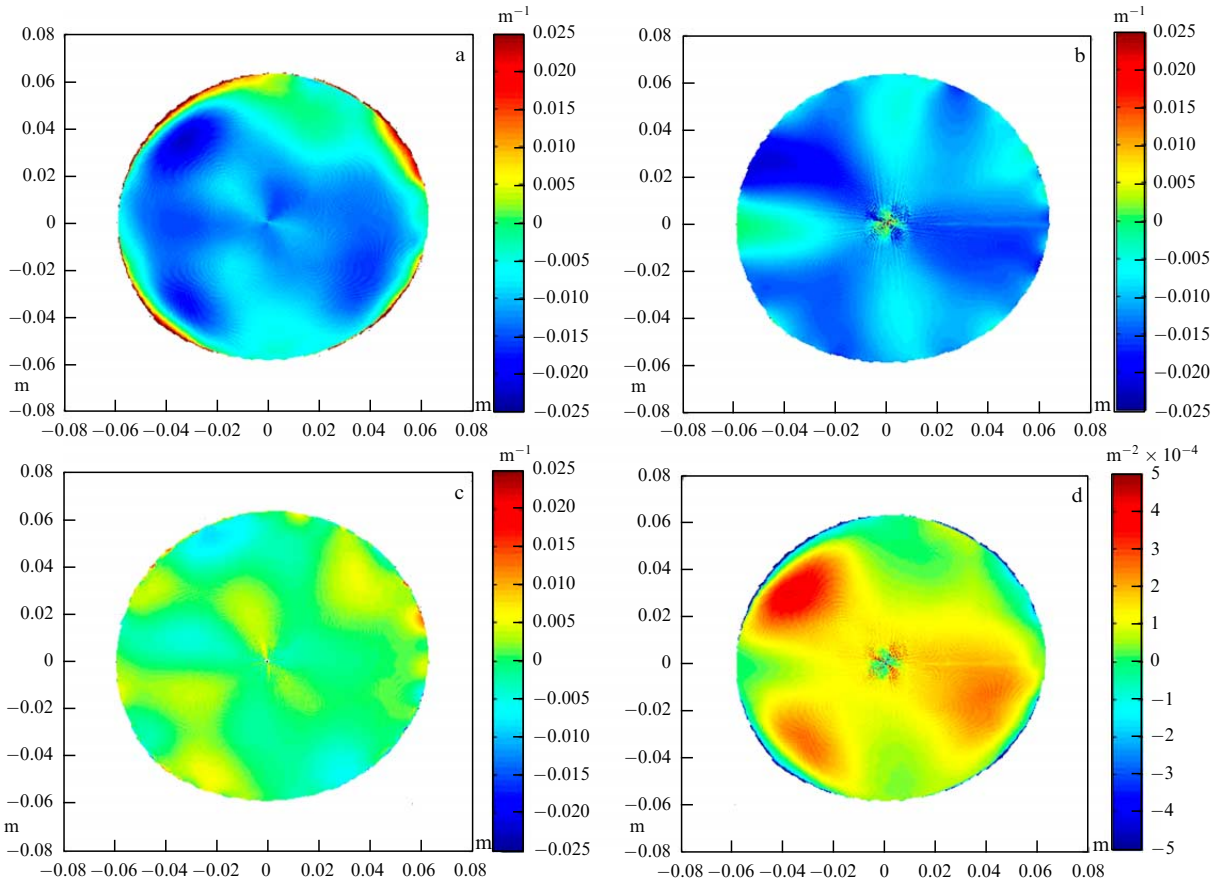

Figure 8. Results of calculations in a cylindrical system of coordinates for the wafer shape close to spherical (topography presented in Fig. 2a): (a) k_{rr}, (b) $k_{\theta\theta}$, (c) $k_{r\theta}$, (d) Gaussian curvature $K = k_{rr}\,k_{\theta\theta}$.

window) or global approximation of the surface by polynomials of a different order.

For example, in the Evans method, a second-order polynomial, whose coefficients are first and second partial derivatives, is fitted by the least-squares method to the 3×3 moving window, for the points of which the Cartesian coordinates and surface elevations are known. Moving the window over the DEM, specified on a square grid, one can calculate the values of partial derivatives and, correspondingly, the values of the local morphometric characteristics for all DEM points, except the edge rows and columns.

By analyzing the sign of the K value, three types of surfaces at a given point are distinguished [85]. The first case is when two principal curvatures k_1 and k_2 ($k_{\min}$ and $k_{\max}$, respectively) are nonzero and have the same sign; the Gaussian curvature K is positive. The corresponding point is called elliptic. The simplest example of such a surface is a sphere.

The second case is when the signs of the principal curvatures k_1 and k_2 are different, which leads to a negative value of the Gaussian curvature K. The corresponding point is called a saddle point [85].

The third case is when one of the principal curvatures is zero, which leads to a zero Gaussian curvature. The corresponding point is parabolic [85]. An example of a surface with such points is the side surface of a cylinder.

The sign of the mean curvature H determines the predominant direction of bending. For convex local regions of a surface, the mean curvature is positive, for concave regions, it is negative, and for locally flat regions, it is zero [87, 88]. Note that, hereinafter, in the description of specific features of morphometric variables, the normal to the surface is considered directed from the surface (see Fig. 10). However, the maps of curvatures (Figs 11 and 12) are obtained with the normal directed to the surface, which leads to a change of the sign of the mean curvature H and the principal curvatures.

It is useful to analyze the principal curvatures, the maximal and minimal ones. It should be taken into account that the maximal curvature is such taking into account the signs of the variables, i.e., in absolute value it can be even smaller than the second principal curvature (if the minimal curvature is negative). In a mainly concave region (with a negative mean curvature), the absolute value of the minimal curvature will be greater than the absolute value of the maximal curvature. Similarly, in a mainly convex region (with a positive mean curvature), the absolute value of the maximal curvature will be greater than that of the minimal curvature.

Positive values of the maximal curvature correspond to extended convex regions of the surface, and negative values, to local concave elements of topography (hollows). Positive values of the minimal curvature correspond to local convex elements (hillocks), while negative values, to extended concave regions on the surface [3].

A detailed description of various surface types (Fig. 13) [90] and the corresponding curvatures is vast [3] and extends beyond the framework of this paper. In essence, the considered mathematical apparatus rather thoroughly describes the surface shape, which determines such fields of its

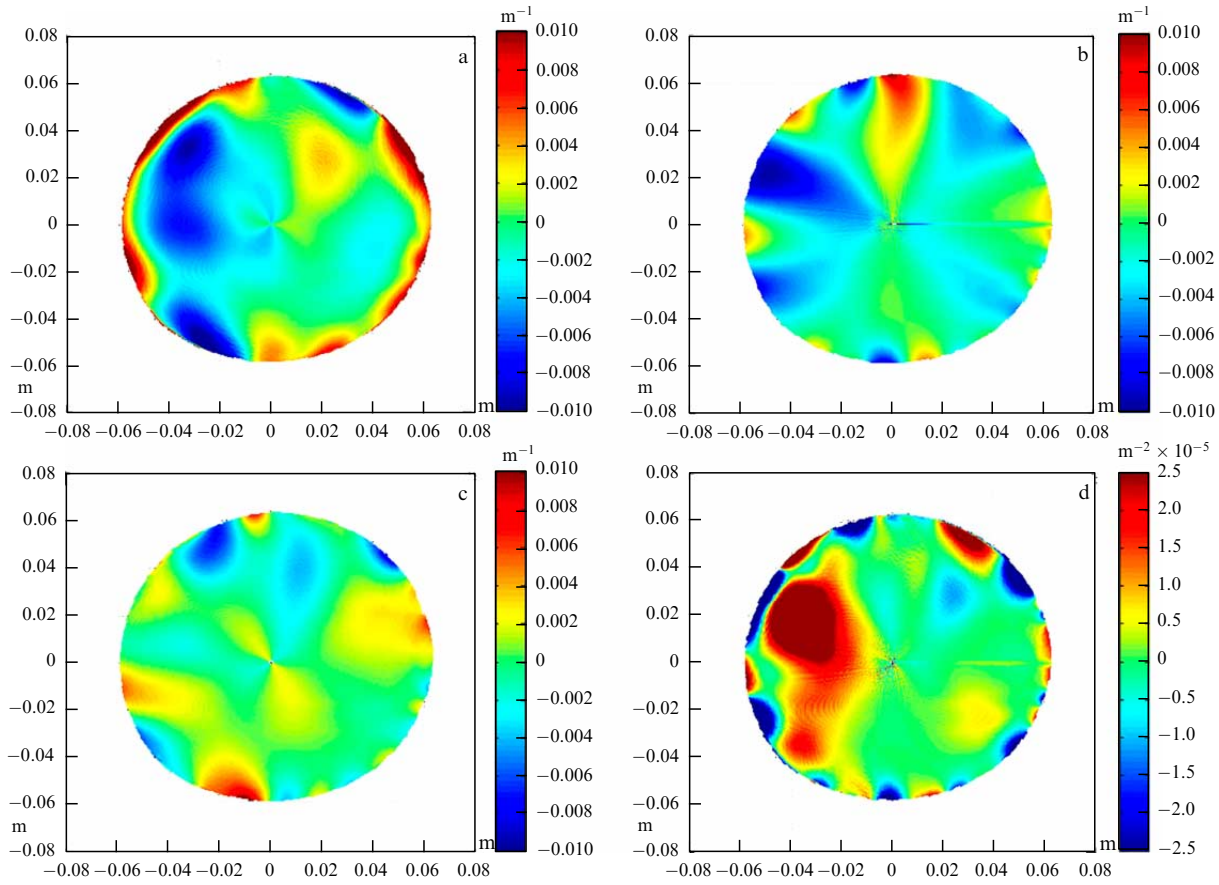

Figure 9. Results of calculations in a cylindrical system of coordinates for the wafer complex shape (topography presented in Fig. 3a): (a) k_{rr}, (b) $k_{\theta\theta}$, (c) $k_{r\theta}$, (d) Gaussian curvature $K = k_{rr}\, k_{\theta\theta}$.

application as the analysis and classification of the shapes of details [91–93], architecture [94], Earth sciences [89], and ophthalmology [95].

Worth separate attention is such a morphometric variable as the curvature intensity [96], or unsphericity [3] (see Table 2). In Ref. [96] a correlation and factor analysis of the curvature parameters was carried out. It was found that the curvature intensity characterizes the specific features of deformation most reliably and adequately. It is also pointed out that the curvature intensity directly depends on the shear strain intensity, related to the maximal shear stress.

There are a number of papers using the notion of Gaussian curvature to analyze the behavior and changes in structure shapes, mainly of bistable systems [70–74, 76, 97–102]. Many of them mention the Gaussian Theorema Egregium that describes the interconnection of Gaussian curvature and strains.

Thus, the mathematical apparatus considered not only allows a qualitative analysis of the surface shape but also is directly related to the important problem of analyzing the mechanical stresses and stability of systems. It is logical to also apply the possibilities available in geomorphometry [103, 104] to the analysis of wafers and small-size objects.

We analyzed the DEMs of the surfaces presented in Figs 2a and 3a. Figures 11 and 12 show the calculated principal curvatures, the mean curvature, and the Gaussian curvature.

The shape of the wafer presented in Fig. 2a is similar to that of a convex segment of a sphere, which corresponds to positive Gaussian curvature and positive mean curvature. By analyzing the maps of principal curvatures (Fig. 11a, b), one

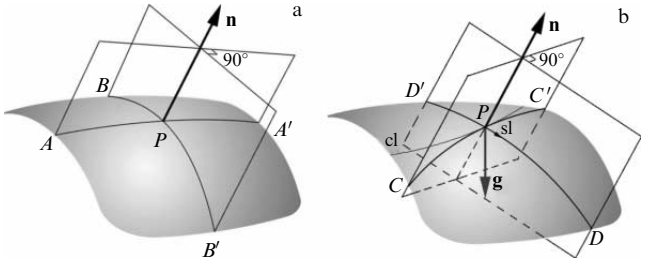

Figure 10. Two pairs of normal sections at point P of a topographic surface: (a) principal sections APA' and BPB', (b) normal sections CPC' and DPD' selected by gravity. **n** is the outer normal to the surface, **g** is the gravity force acceleration vector, cl is the contour line, sl is the slope line [3].

can determine the local regions with greater and smaller curvature and the corresponding topographic features. The comparability of data of maps in Figs 4b, 6a, 8a, and 11a is evident.

The wafer shape presented in Fig. 3a is rather complex. There are vast-area convex and concave regions (see Fig. 12). Overall, the maps presented in Fig. 12 are much more informative than the data presented in Fig. 3a and allow localizing sites by different features. The minimal curvature is good for localizing extended concave surface regions; it also indicates the position of a few 'hillocks' (convex regions). The maximal curvature shows another localization level, e.g., one can see a convex section within a mainly concave extended region. The principal curvatures are independent of each

Table 2. Definitions, formulas, and interpretations of geomorphometric variables constituting a complete system of surface curvatures [3, 86, 87].

Name	Notation, unit of measurement	Expression, definition, and brief interpretation
Form attributes		
Minimal curvature	$k_{\min}$ or k_1, m^{-1}	$k_{\min} = H - M$ Curvature of the principal normal section (Fig. 10a) with the minimal bend at a given point of a topographic surface. In the geomorphological sense, positive values of the minimal curvature indicate local convex topography elements, and negative ones indicate valleys.
Maximal curvature	$k_{\max}$ or k_2, m^{-1}	$k_{\max} = H + M$ Curvature of the principal normal section (Fig. 10a) with the maximal bend at a given point of a topographic surface. In the geomorphological sense, positive values of the maximal curvature indicate ridges, and negative ones indicate local wells.
Mean curvature	H, m^{-1}	$H = \frac{1}{2}(k_{\min} + k_{\max}) = \frac{1}{2}(k_{\mathrm{h}} + k_{\mathrm{v}}) = -\frac{(1+k_y^2)k_{xx} - 2k_xk_yk_{xy} + (1+k_x^2)k_{yy}}{2\sqrt{(1+k_x^2+k_y^2)^3}}$ Half-sum of any two normal mutually perpendicular sections at a given point of a topographic surface. Represents two mechanisms of flow accumulation, the convergence and the relative deceleration, with equal weights.
Gaussian curvature	K, m^{-2}	$K = k_{\min}k_{\max} = \frac{k_{xx}k_{yy} - k_{xy}^2}{(1+k_x^2+k_y^2)^2}$ Product of the maximal and minimal curvatures. According to *Theorema Egregium*, the Gaussian curvature of a surface preserves its values after its bending if it occurred without stretching, compressions, or disruptions.
Unsphericity	M, m^{-1}	$M = \frac{1}{2}(k_{\max} - k_{\min}) = \sqrt{H^2 - K}$ Half-difference of the maximal and minimal curvatures. $M = 0$ on a sphere. Shows the deviation of Earth's surface element shape from spherical.
Flow attributes		
Vertical curvature	k_{v}, m^{-1}	$k_{\mathrm{v}} = -\frac{k_x^2k_{xx} + 2k_xk_yk_{xy} + k_y^2k_{yy}}{(k_x^2+k_y^2)\sqrt{(1+k_x^2+k_y^2)^3}}$ Curvature of the normal section having a common tangent with the slope line (Fig. 10b) at a given point of a topographic surface. A measure of relative deceleration of flows moving along the surface under the action of gravity (one of two mechanisms of flow accumulation). The flows decelerate at $k_{\mathrm{v}} < 0$ and accelerate at $k_{\mathrm{v}} > 0$. In the geomorphological sense, maps of vertical curvature can help to distinguish terrace levels.
Horizontal curvature	k_{h}, m^{-1}	$k_{\mathrm{h}} = -\frac{k_y^2k_{xx} - 2k_xk_yk_{xy} + k_x^2k_{yy}}{(k_x^2+k_y^2)\sqrt{1+k_x^2+k_y^2}}$ Curvature of the normal section tangent to the contour line (Fig. 10b) at a given point of a topographic surface. A measure of convergence of the flows moving over the surface subjected to gravity (one of two flow accumulation mechanisms). The flows converge at $k_{\mathrm{h}} < 0$ and diverge at $k_{\mathrm{h}} > 0$. In the geomorphological sense, maps of the horizontal curvature emphasize offspurs of ridges and valleys (the regions of divergence and convergence, respectively).
Difference curvature	E, m^{-1}	$E = \frac{1}{2}(k_{\mathrm{v}} - k_{\mathrm{h}})$ Half-difference of vertical and horizontal curvatures. Shows how strongly expressed is one of two mechanisms of accumulation: the relative deceleration of flows (for which k_{v} is responsible) compared to another mechanism, the convergence of flows (for which k_{h} is responsible), at a given point on the topographic surface.
Horizontal excess curvature	k_{he}, m^{-1}	$k_{\mathrm{he}} = k_{\mathrm{h}} - k_{\min} = M - E$ Difference between horizontal and minimal curvatures. Shows how strongly the normal section tangent to the horizontal is bent compared to the minimal bend of the topographic surface at a given point.
Vertical excess curvature	k_{ve}, m^{-1}	$k_{\mathrm{ve}} = k_{\mathrm{v}} - k_{\min} = M + E$ Difference between vertical and minimal curvatures. Shows how much stronger the normal section having a common tangent with the slide line is bent than the minimal bend of the topographic surface at a given point.

Table 2. (continued)

Name	Notation, unit of measurement	Expression, definition, and brief interpretation
Accumulation curvature	K_a, m^{-2}	$K_a = k_h k_v = H^2 - E^2$ Product of vertical and horizontal curvatures. Can be used to assess the degree of flow accumulation.
Ring curvature	K_r, m^{-2}	$K_r = k_{he} k_{ve} = M^2 - E^2$ Product of horizontal excess and vertical excess curvatures. Describes the degree of flow tortuosity.

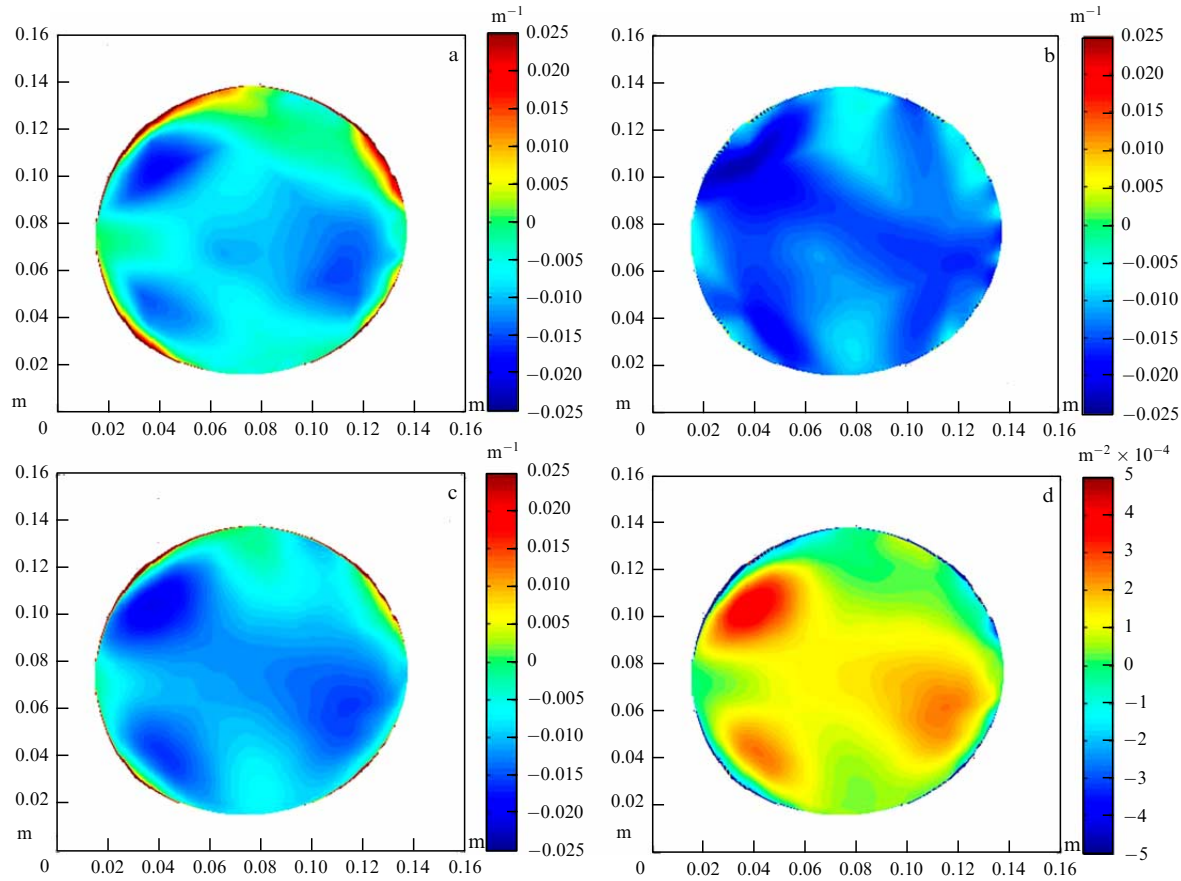

Figure 11. Results of calculating principal (k_{max} and k_{min}), mean (H), and Gaussian (K) curvatures for the wafer shape close to spherical (topography presented in Fig. 2a): (a) k_{max}, (b) k_{min}, (c) H, (d) K.

other [94] and, according to Fig. 10, simultaneously characterize the surface at different levels.

It is worth taking into account that the values along the Z-axis are a few orders of magnitude smaller than those along X and Y. Therefore, to shift the accent in the analysis and to provide better clarity of presentation, it is possible to replace the initial data set (x_i, y_i, z_i) with the data set (x_i, y_i, Cz_i), C being a factor large enough to make the values along the Z-axis substantially greater than those along X and Y.

In addition, since the morphometric variables usually have a wide dynamical range of values, in order to avoid the loss of information about their spatial distribution, the mapping in geomorphometry is performed using the following logarithmic transformation [3]:

$$\tilde{\Upsilon} = \operatorname{sign} \Upsilon \ln \left(1 + 10^{\hat{n}\hat{m}} |\Upsilon|\right), \qquad (7)$$

where $\tilde{\Upsilon}$ and Υ are the transformed and the initial values of a morphometric variable, respectively, $\hat{n} = 0$ for nonlocal variables, $\hat{n} = 2, \ldots, 9$ for local variables, $\hat{m} = 2$ for K, K_a, and K_r, and $\hat{m} = 1$ for other variables. The choice of $\hat{n}$ depends on the DEM grid size.

We specially note that the technique described in this section is efficient in the analysis of complex-shaped structures having a slope. Practically, one has to deal with the necessity of preprocessing the measurement results, including the elimination of a linear slope. However, in the case of a complex shape of the object under study, the calculation of the plane to be subtracted often becomes a nontrivial task and requires time, mastery, and a creative approach on the part of the researcher. The linear slope is not an obstacle to the correct curvature calculation by geomorphometry methods; therefore, these maps are proposed for use in DEM analysis.

The maps of Gaussian curvature calculated in the cylindrical [76, 105] and Cartesian coordinate systems are generally comparable (Figs 6d, 8d, and 11d; Figs 7d, 9d, and 12d). However, in the central part of the maps calculated in the cylindrical system of coordinates, artifacts are observed (see Figs 8 and 9). They arise because the origin of coordinates

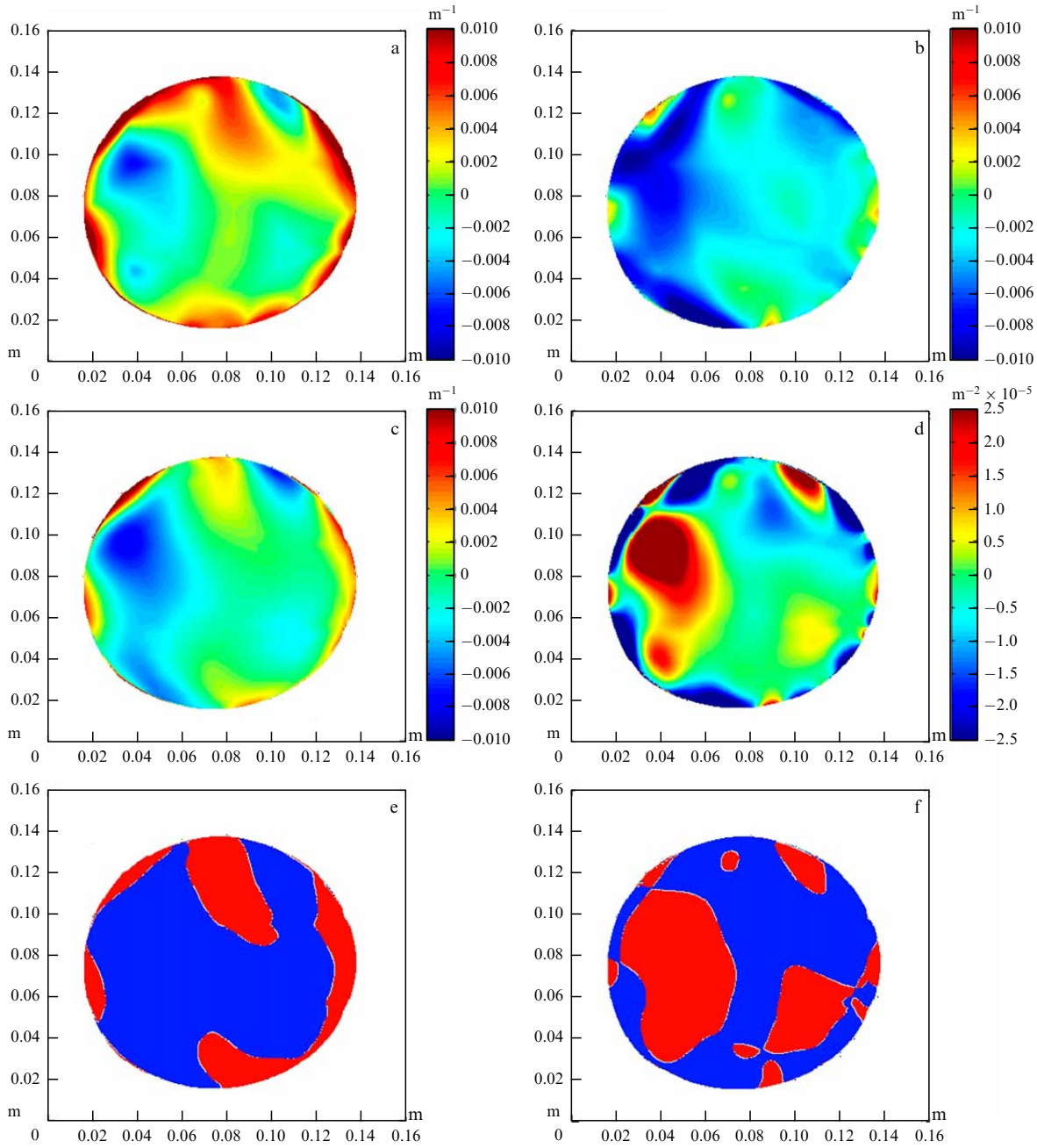

Figure 12. (Color online.) Results of calculating the principal (k_{max} and k_{min}), mean (H), and Gaussian (K) curvatures for the complex-shaped wafer (topography presented in Fig. 3a): (a) k_{max}, (b) k_{min}, (c) H, (d) K, (e) sign of H (dark blue for $H < 0$, light red for $H > 0$), (f) sign of K (dark blue for $K < 0$, light red for $K > 0$).

(pole) in the cylindrical coordinate system is a point of singularity: one of the coordinates (the angle) is indefinite at this point. Upon interpolating from a square grid of a Cartesian coordinate system to the radial concentric mesh of the cylindrical coordinate system, a discontinuity of the function z takes place around the pole of the latter, and the Gibbs phenomenon arises in the pole neighborhood (characteristic spikes of the function near the discontinuity point) [106]. The spike amplitudes are not large, and in the topography (elevation) map they are not noticeable to the user. However, after calculating the derivatives and the Gaussian curvature, such artifacts become noticeable. This is quite natural, since it is well known that derivatives are very sensitive to HF noise, and, the higher the derivative order, the higher the sensitivity [106]. Attempts to counter this effect are possible using stretched splines for interpolation [107] or rarefying the radial concentric DEM mesh near the pole. However, complete elimination of these artifacts is impossible.

Although some researchers use in calculations the approximate (simplified) expression for the Gaussian curvature $\hat{K} = k_{xx}k_{yy} - k_{xy}^2$ [101] (i.e., the first derivatives are assumed to be zero), for the wafers under study, the maps of the Gaussian curvature, calculated using this expression, are on the whole similar to those of the Gaussian curvature obtained by the standard calculation through principal curvatures.

The calculated Gaussian curvatures in the Cartesian and cylindrical coordinate systems using the geomorphometry methods are on the whole similar (Figs 6d, 8d, and 11d;

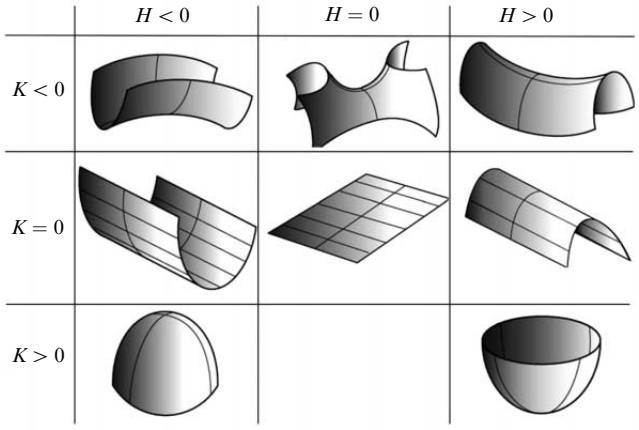

Figure 13. Schematic diagrams for the Gaussian classification of surface shapes [90].

Figs 7d, 9d, and 12d). This observation testifies to the correctness of each of the described techniques, in spite of the peculiarities related to performing numerical computations with different software (computation errors) and the presence of a series of transformations of the experimental data (reconstruction of missing data, if necessary, correction of the dimension of the processed array, flattening, interpolation, etc.).

Overall, the geomorphometry methods are efficient for localization of different types of surface regions, which is often hard to implement by a purely visual analysis of the wafer surface topography.

In spite of the relatively rare application of the variables described in this section to the analysis of structures in microelectronics, it is possible to expect more attention to this field of knowledge. This is due to the necessity of careful control of the topographic features when performing technological operations with wafers, e.g., in bonding the wafers or studying thickened wafers. Moreover, the approaches described in this paper can be implemented not only for the analysis of the topography of round wafers, but also for calculating the curvature of small-size structures, including MEMS [9, 108–112]. They can be also applied for subsequent calculation of the stress tensor [86].

7. Conclusion

Three ideologically close approaches to curvature determination in wafers from their surface shape are described. The application of these approaches is demonstrated by the example of wafers with a simple-shaped surface (a spherical segment with a curvature radius of about 80 m), as well as complex-shaped ones (with convex and concave regions). Maps of distributions (over the surface profiles) are presented for the curvature and the curvature radius, the partial derivatives k_{xx}, k_{yy}, k_{xy}, k_{rr}, $k_{\theta\theta}$, $k_{r\theta}$, and the principal, mean, and Gaussian curvatures.

The approach based on the analysis of surface profiles, especially using second-order polynomials for approximation, is efficient in operating with a large number of wafers having a simple (spherical) shape, when it is required to perform fast measurements and calculate mechanical stresses, to compare the samples with each other. What is more, in connection with the automation of production and measurement processes, as well as the necessity of a more careful analysis of structures, the techniques based on the analysis of surface profiles can only be considered to be gradually becoming obsolescent.

Using the curvature or curvature radius for the analysis depends on the range of the analyzed values — it may be convenient to operate with the quantity itself as well as with its reciprocal.

Depending on the purpose of the subsequent processing and on the specific features of the object analyzed (the presence of central symmetry), a Cartesian or cylindrical system of coordinates can be used. However, the use of the cylindrical system of coordinates in calculations gives rise to unremovable artifacts. Since the analysis of realistic structures does not imply their symmetry, the advantage of calculations in the cylindrical system of coordinates is offset.

The vast mathematical toolkit of geomorphometry seems most promising for the analysis of surface topography irregularities, since the calculated morphometric variables have a clear physical meaning and are easily interpretable.

Using both the second derivatives in coordinates and the curvatures calculated from differential geometry is well suited to calculating mechanical stresses.

This paper does not nearly describe all the possible options for determining the curvature of a wafer surface. However, even the presented approaches substantially extend the spectrum of information obtained by analyses.

Acknowledgments. The authors are grateful to V Yu Kireev (Zelenograd Nanotechnology Center), S A Lychev (Ishlinsky Institute for Problems in Mechanics, RAS), and N V Bogachev (Skoltech, Moscow Institute of Physics and Technology, National Research University) for their discussions and valuable comments.

The work was carried out using the equipment at the MIET Core facilities center ''MEMS and electronic components'' as part of the implementation of the program of the Leading Research Center, Trusted Sensor Systems (contract no. 009/20 dated April 10, 2020). The work of A A D and N A D was carried out with financial support from the Ministry of Telecoms and Mass Communications of Russia and the Russian Venture Company (subsidy agreement identifier 0000000007119R190002).

References

1. Dyuzhev N A et al. *Nanotechnol. Russia* **12** 426 (2017); *Ross. Nanotekhnol.* **12** (7–8) 97 (2017)
2. Gusev E E et al. *Nano- Mikrosist. Tekh.* **19** 331 (2017)
3. Florinsky I V *Digital Terrain Analysis in Soil Science and Geology* 2nd ed. (Amsterdam: Elsevier. Academic Press, 2016)
4. Kirillovskii V K, Tochilina T V *Opticheskie Izmereniya* (Optical Measurements) Pt. 1 *Izmereniya Geometricheskikh Parametrov* (Measurements of Geometric Parameters) 2nd ed., ster. (St. Petersburg: ITMO, 2015)
5. Kirillovskii V K*Opticheskie Izmereniya* (Optical Measurements) Pt. 3 *Funktsional'naya Skhema Pribora Opticheskikh Izmerenii. Tipovye Uzly. Opticheskie Izmereniya Geometricheskikh Parametrov* (Functional Diagram of an Optical Measurement Device. Standard Units. Optical Measurements of Geometric Parameters) (St. Petersburg: ITMO, 2005)
6. Malacara D (Ed.) *Optical Shop Testing* (New York: Wiley, 1978); Translated into Russian: *Opticheskii Proizvodstvennyi Kontrol'* (Moscow: Mashinostroenie, 1985)
7. Djuzhev N A et al. *IOP Conf. Ser. Mater. Sci. Eng.* **189** 012019 (2017)
8. Yun H M, Chao L P, Hsu J S *Appl. Mech. Mater.* **121–126** 4295 (2012)

9. Poelma R H et al. *J. Micromech. Microeng.* **21** 065003 (2011)
10. Dunn M L, Zhang Y, Bright V M *J. Microelectromech. Syst.* **11** 372 (2002)
11. Pilipenko V A et al. *Prib. Metody Izmer.* (1) 71 (2011)
12. Egorov G P "Mekhanicheskie napryazheniya v metallicheskikh plenkakh pri magnetronnom osazhdenii" ("Mechanical stresses in metallic films under magnetron deposition"), Ph.D Thesis (Phys.-Math. Sci.) (Moscow: MISIS, 2018)
13. Sen'ko S F, Zelenin V A *Prib. Metody Izmer.* **9** 74 (2018)
14. Sen'ko S F, Sen'ko A S, Zelenin V A *Dokl. Beloruss. Gos. Univ. Inform. Radioelektron.* (5) 12 (2018)
15. Freund L B, Suresh S *Thin Film Materials. Stress, Defect Formation, and Surface Evolution* (Cambridge: Cambridge Univ. Press, 2003)
16. Vaudin M D, Kessler E G, Owen D M *Metrologia* **48** 201 (2011)
17. Rosakis A J et al. *Thin Solid Films* **325** 42 (1998)
18. van Dijk L et al. *Proc. SPIE* **10145** 101452L (2017)
19. Dong X et al. *Opt. Express* **19** 13201 (2011)
20. Dong X et al. *Exp. Mech.* **53** 959 (2013)
21. Zhang C et al. *Exp. Mech.* **56** 1123 (2016)
22. Stoney G G *Proc. R. Soc. Lond. A* **82** 172 (1909)
23. Aivazyan G E *Izv. Nats. Akad. Nauk Resp. Armeniya Gos. Inzh. Univ. Armenii Ser. Tekh. Nauk* **53** 63 (2000)
24. Dedkova A A, Kireev V Yu, Makhiboroda M A *Nanostrukt. Matem. Fiz. Model.* **20** (2) 23 (2020)
25. Tabenkin A N, Tarasov S B, Stepanov S N *Sherokhovatost', Volnistost', Profil'. Mezhdunarodnyi Opyt* (Roughness, Waviness, Profile. International Experience) (St. Petersburg: Izd. Politekhnicheskogo Univ., 2007)
26. Glang R, Holmwood R A, Rosenfeld R L *Rev. Sci. Instrum.* **36** 7 (1965)
27. Novak A V, Novak V R, Dedkova A A, Gusev E E *Semiconductors* **52** 1953 (2018); *Izv. Vyssh. Uchebn. Zaved. Elektron.* **22** 138 (2017)
28. Bigl S et al. *Materials* **10** 1287 (2017)
29. Dobrynin A V *Tech. Phys. Lett.* **23** 709 (1997); *Pis'ma Zh. Tekh. Fiz.* **23** (18) 32 (1997)
30. Markochev V M, Egorov G P *Zavod. Lab. Diagnost. Mater.* **84** (3) 61 (2017)
31. Ohlidal I et al. *Proc. SPIE* **5527** 139 (2004)
32. Mallik A, Stout R, Ackaert J *IEEE Trans. Components Packag. Manuf. Technol.* **4** 240 (2014)
33. Strunin V I, Khudaibergenov G Zh, in *Omskie Nauchnye Chteniya — 2018. Materialy Vtoroi Vserossiiskoi Nauchnoi Konf., Omsk, 10–15 Dekabrya 2018 g.* (Omsk Scientific Readings — 2018. Proc. of the Second All-Russian Scientific Conf., Omsk, December 10–15, 2018) (Exec. Ed. T F Yashchuk) (Omsk: Omsk. Gos. Univ. im. F.M. Dostoevskogo, 2018) p. 644
34. Picciotto A et al. *Appl. Surf. Sci.* **256** 251 (2009)
35. Stenzel O et al. *Thin Solid Films* **517** 6058 (2009)
36. Szekeres A, in *Fundamental Aspects of Ultrathin Dielectrics on Si-based Devices* (NATO Science Series, Vol. 47, Eds E Garfunkel, E Gusev, A Vul') (Dordrecht: Springer, 1998) p. 65, https://doi.org/10.1007/978-94-011-5008-8_5
37. Bouaouina B et al. *Surf. Coat. Technol.* **333** 32 (2018)
38. Klose Ph et al. *Int. J. Hydrogen Energy* **42** 22583 (2017)
39. Seidl W M et al. *Surf. Coat. Technol.* **347** 92 (2018)
40. Krawiec H et al. *Appl. Surf. Sci.* **475** 162 (2019)
41. Sen'ko S F, Zelenin V A *Prib. Metody Izmer.* **9** 254 (2018)
42. Shinohara A et al. *Mater. Sci. Forum* **941** 2069 (2018)
43. Liu D, Chen W *J. Eng. Mater. Technol.* **134** 031002 (2012)
44. Liu D Y, Chen W Q *Mech. Res. Commun.* **37** 520 (2010)
45. Wang T-G et al. *Mater. Sci. Eng. A* **527** 454 (2010)
46. Zhang N-H, Chen J-Z *Eur. J. Mech. A* **28** 284 (2009)
47. Zhang X C et al. *Surf. Coat. Technol.* **201** 6715 (2007)
48. Klein C A, Miller R P *J. Appl. Phys.* **87** 2265 (2000)
49. Benabdi M, Roche A A *J. Adhesion Sci. Technol.* **11** 281 (1997)
50. Kovalenko D A, Petrov V V *Zh. Nano- Elektron. Fiz.* **7** 03036 (2015)
51. Chou T-L, Yang S-Y, Chiang K-N *Thin Solid Films* **519** 7883 (2011)
52. Joseph S et al. *Proc. SPIE* **9453** 94530R (2015)
53. But D K, Bychkov P S, Lychev S A *Vestn. Perm. Nats. Issled. Politekh. Univ. Mekh.* (1) 17 (2020)
54. Bychkov P S, Lychev S A, But D K *Vestn. Samar. Univ. Estestvennonauchn. Ser.* **25** (4) 48 (2019)
55. Dedkova A A et al. *Russ. J. Nondestruct. Testing* **56** 452 (2020); *Defektoskopiya* (5) 52 (2020)
56. Djuzhev N A et al. *IOP Conf. Ser. Mater. Sci. Eng.* **289** 012007 (2018)
57. Jiang C et al. *Proc. SPIE* **10932** 109320K (2019)
58. Mao C-L et al. *Acta Metrolog.* **39** 5628 (2018)
59. Ardigo M R, Ahmed M, Besnard A *Adv. Mater. Res.* **996** 361 (2014)
60. Borgardt N I, Alekseev N V, Volkov R L *Izv. Vyssh. Uchebn. Zaved. Elektron.* (5) 91 (2011)
61. Guzhov V et al. *Avtomatika Programmnaya Inzh.* (2) 71 (2016)
62. Loparev A V et al. *J. Opt. Technol.* **79** 371 (2012); *Opt. Zh.* **79** (6) 79 (2012)
63. Dedkova A A, Makhiboroda M A *Nanostrukt. Matem. Fiz. Model.* **20** (2) 41 (2020)
64. Zentsova E A, in *Innovatsii, Kachestvo i Servis v Tekhnike i Tekhnologiyakh. V Mezhdunarodnaya Nauchno-prakticheskaya Konf., 04–05 Iyunya 2015 g. Sbornik Nauchnykh Trudov* (Innovation, Quality and Service in Engineering and Technology. V International Scientific and Practical Conference, June 04–05, 2015. Collection of Scientific Papers) (Kursk: Yugo-Zapadnyi Gos. Univ. 2015) p. 150
65. Kireev V Yu, Stolyarov A A *Tekhnologii Mikroelektroniki. Khimicheskoe Osazhdenie iz Gazovoi Fazy* (Technologies of Microelectronics. Chemical Vapor Deposition) (Moscow: Tekhnosfera, 2006)
66. Ivanov A O, Tuzhilin A A "Lektsii po klassicheskoi differentsial'noi geometrii" ("Lectures on classical differential geometry"), http://dfgm.math.msu.su/files/IvaTuzTerm1-2017.pdf
67. Skopenkov A B *Osnovy Differentsial'noi Geometrii v Interesnykh Zadachakh* (Fundamentals of Differential Geometry in Interesting Problems) (Moscow: MTsNMO, 2009)
68. Huang Y, Ngo D, Rosakis A J *Acta Mech. Sinica* **21** 362 (2005)
69. Kiyamov Kh G et al. *Izv. Kazan. Gos. Arkhitekturno-stroitel'nogo Univ.* (1) 35 (2007)
70. Seffen K A, Guest S D *J. Appl. Mech.* **78** 011002 (2011)
71. Seffen K A, McMahon R A *Int. J. Mech. Sci.* **49** 230 (2007)
72. Guest S D, Kebadze E, Pellegrino S *J. Mech. Mater. Struct.* **6** 203 (2011)
73. Eckstein E, Pirrera A, Weaver P M *AIAA J.* **54** 1778 (2016)
74. Seffen K A *J. Appl. Mech.* **83** 021005 (2016)
75. Sobota P M, Seffen K A *R. Soc. Open Sci.* **6** 190888 (2019)
76. Sobota P M, Seffen K A *Proc. R. Soc. Lond. A* **473** 20170230 (2017)
77. Wang M Q et al. *Int. J. Solids Struct.* **49** 1701 (2012)
78. Ngo D et al. *Thin Solid Films* **515** 2220 (2006)
79. Brown M A "Measuring stress in thin film - substrate systems featuring spatial nonuniformities of film thickness and/or misfit strain", Thesis in partial fulfillment of the requirements for the degree of Doctor of Philosophy (Pasadena, CA: California Inst. of Technology, 2007)
80. Leksin A Yu, Kutrovskaya S V *Fizicheskie i Matematicheskie Printsipy Adaptivnoi Optiki* (Physical and Mathematical Principles of Adaptive Optics) (Vladimir: VlGU, 2015) Guidelines for laboratory training of VlSU students studying in the fields 12.02.05 'Laser engineering and laser technologies', 12.04.02 'Optotechnics', 12.04.05 'Laser engineering and laser technologies'
81. Tvorogov S "Sage: stroim polinomy Zernike" ("Sage: constructing Zernike polynomials"), https://sergeitvorogov.ru/archives/2376
82. Zernike F *Physica* **1** 689 (1934)
83. Poznyak E G, Shikin E V *Differentsial'naya Geometriya*: *Pervoe Znakomstvo* (Differential Geometry: First Acquaintance) (Moscow: Izd. MGU, 1990)
84. Kuznetsova E V *Stroitel'naya Mekhanika. Izgib Plastin* (Building Mechanics. Bending of Plates) (Perm: Permskii Gos. Tekh. Univ., 2006) A tutorial
85. Pogorelov A V *Differentsial'naya Geometriya* (Differential Geometry) (Moscow: Nauka, 1974)
86. Machado G, Favier D, Chagnon G *Exp. Mech.* **52** 865 (2012)
87. Shary P A *Math. Geol.* **27** 373 (1995)
88. Shary P A, Sharaya L S, Mitusov A V *Geoderma* **107** 1 (2002)
89. Florinsky I V *Prog. Phys. Geogr. Earth Environment* **41** 723 (2017)
90. Mynatt I, Bergbauer S, Pollard D D *J. Struct. Geol.* **29** 1256 (2007)
91. Radzevich S P *Formoobrazovanie Poverkhnostei Detalei* (*Osnovy Teorii*) (Formation of Surfaces of Parts (Fundamentals of Theory)) (Kiev: Rastan, 2001)

92. Ponomarev B B, Nguyen Shi Hien *Vestn. Irkutsk. Gos. Tekh. Univ.* **22** (4) 62 (2018)
93. Nguyen Shi Hien *Novaya Nauka Sovrem. Sost. Puti Razvitiya* (12-4) 99 (2016)
94. Pellis D, Pottmann H, in *Advances in Architectural Geometry 2018* (Eds L Hesselgren) (Vienna: Klein Publ. GmbH, 2018) p. 34
95. R-Optics, https://r-optics.ru/product/analizator-perednego-segmenta-glaza-pentacam-5002
96. Grachev A V, Mukhamediev Sh A, Nikolaev V A *Russ. J. Earth Sci.* **2** (1) RJE00034 (2000)
97. Pezzulla M et al. *Soft Matter* **12** 4435 (2016)
98. Wang H, Nilsen E T, Upmanyu M *J. R. Soc. Interface* **17** 20190751 (2020)
99. Seffen K A, Maurini C *J. Mech. Phys. Solids* **61** 190 (2013)
100. Fernandes A, Maurini C, Vidoli S *Int. J. Solids Struct.* **47** 1449 (2010)
101. Hamouche W et al. *Meccanica* **51** 2305 (2016)
102. Hamouche W et al. *Proc. R. Soc. Lond. A* **473** 20170364 (2017)
103. Pike R J *Int. J. Machine Tools Manuf.* **41** 1881 (2001)
104. Pike R J *Prof. Geogr.* **53** 263 (2001)
105. Stepanenko V A, Okhotkin K G, Zakharov Yu V *Differentsial'naya Geometriya* (Differential Geometry) Pt. 1 *Metodicheskie Ukazaniya po Kursu 'Matematicheskii Analiz' dlya Studentov Fizicheskogo Fakul'teta i Mezhvuzovskogo Inzhenerno-fizicheskogo Otdeleniya* (Guidelines for the Course 'Mathematical Analysis' for Students of the Faculty of Physics and Interuniversity Engineering Physics Department) (Krasnoyarsk: Krasnoyarsk. Gos. Univ., 2000); http://sibsauktf.ru/courses/DiffGeom/
106. Florinsky I V *Int. J. Geogr. Inf. Sci.* **16** 475 (2002)
107. Mitášová H, Mitáš L *Math. Geol.* **25** 641 (1993)
108. Favache A et al. *Rev. Sci. Instrum.* **87** 015002 (2016)
109. Djuzhev N A et al. *Proc. SPIE* **10224** 1022428 (2016)
110. Dedkova A A et al. *Nanostrukt. Matem. Fiz. Model.* **17** (1) 51 (2017)
111. Poelma R H et al. *J. Micromech. Microeng.* **21** 065003 (2011)
112. Laconte J et al. *Microelectron. Eng.* **76** 219 (2004)